Nanoporous separators for supercapacitor using activated carbon monolith electrode from oil palm empty fruit bunches

N. S. M. Nor, M. Deraman, R. Omar, E. Taer, Awitdrus, R. Farma, N. H. Basri, and B. N. M. Dolah

Citation: AIP Conference Proceedings **1586**, 68 (2014); doi: 10.1063/1.4866732
View online: http://dx.doi.org/10.1063/1.4866732
View Table of Contents: http://scitation.aip.org/content/aip/proceeding/aipcp/1586?ver=pdfcov
Published by the AIP Publishing

Nanoporous Separators for Supercapacitor Using Activated Carbon Monolith Electrode from Oil Palm Empty Fruit Bunches

N. S. M. Nor[1], M. Deraman*[1], R. Omar[1], E. Taer[2], Awitdrus[2], R. Farma[2], N. H Basri[1], and B. N. M. Dolah[1]

[1]*School of Applied Physics, Faculty of Science and Technology, Universiti Kebangsaan Malaysia, 43600 Bangi, Selangor, Malaysia*
[2]*Department of Physics, Faculty of Mathematics and Natural Sciences, University of Riau, 28293 Pekanbaru, Riau, Indonesia*
**Corresponding author. madra@ukm.my*

Abstract. Activated porous carbon electrode prepared from fibres of oil palm empty fruit bunches was used for preparing the carbon based supercapacitor cells. The symmetrical supercapacitor cells were fabricated using carbon electrodes, stainless steel current collector, H_2SO_4 electrolyte, and three types of nanoporous separators. Cells A, B and C were fabricated using polypropylene, eggshell membrane, and filter paper, respectively. Electrochemical characterizations data from Electrochemical Impedance Spectroscopy, Cyclic Voltammetry, and Galvanic Charge Discharge techniques showed that specific capacitance, specific power and specific energy for cell A were 122 F g^{-1}, 177 W kg^{-1}, 3.42 Wh kg^{-1}, cell B; 125 F g^{-1}, 179 W kg^{-1}, and 3.64 Wh kg^{-1}, and cell C; 180 F g^{-1}, 178 W kg^{-1}, 4.27 Wh kg^{-1}. All the micrographs from Field Emission Scanning Electron Microscope showed that the different in nanoporous structure of the separators lead to a significant different in influencing the values of specific capacitance, power and energy of supercapacitors, which is associated with the mobility of ion into the pore network. These results indicated that the filter paper was superior than the eggshell membrane and polypropylene nanoporous separators. However, we found that in terms of acidic resistance, polypropylene was the best nanoporous separator for acidic medium.

Keywords: Supercapacitor, nanoporous, membrane, carbon, electrode.
PACS: 82.47.Uv, 78.67.Rb, 82.45.Mp, 81.05.U-, 82.45.Fk

INTRODUCTION

Supercapacitor is an energy storage device which finds application in various sectors of technology such as automotive, military, aeronautics and computer, etc. Its major components are electrodes, separator, current collector and electrolyte and it can stores energy based on accumulation of electrostatic charges at the electrode/electrolyte interface. The performance of supercapacitor depends on the properties of its major components [1]. For carbon based supecapacitor, it is important to use highly porous carbon electrodes having pore size, structure and network which are compatible with the size of electrolyte ions; to ensure that the highest possible numbers of ions are accumulated at almost all available pore walls in the electrodes. In order to achieve this condition, different types of supercapacitor activated carbon electrodes (paste [2], fiber-cloth [3], fibre-sheet [4], composite [5-7], film [8], monolith [9, 10]) have been developed and tested in different types of conventional electrolytes (Na_2SO_4, H_2SO_4, KOH etc.) or newly developed electrolytes. Beside active research activities in developing high surface area electrodes and high efficient electrolytes, there has also been growing research activities in developing supercapacitor separators; covering materials such as polypropylene [11], eggshell membrane [12], polyvinyl alcohol (PVA) [13], filter paper [14] and Teflon ring [5-7].

In the present study, three different types of separators namely egg shell membrane, polypropylene and filter paper were used as separator in symmetrical supercapacitor cells fabricated using H_2SO_4 electrolyte and activated carbon electrode prepared from fibres of oil palm empty fruit bunches (EFB). In our previous studies on supercapacitor based on activated carbon monoliths (ACMs) electrodes from EFB [5-7] and rubber wood saw dust (RWSD) [9], Teflon ring

5th Nanoscience and Nanotechnology Symposium (NNS2013)
AIP Conf. Proc. 1586. 68-73 (2014); doi: 10.1063/1.4866732
978-0-7354-1218-7/$30.00

separator [10] was used in the fabrication of cells. The present study, reports the first time usage of polypropylene (PPC), egg shell membrane (ESM) and filter paper (FPW) materials as nanoporous separators in supercapacitor cells based on EFB and RWSD ACMs electrodes. These polypropylene, egg shell membrane and filter paper are known to have nano-pores structure that capable of retaining high amount of electrolyte, and the main objective of the present study is to relate the effect of nano-pores structure characteristics of these separators with the electrochemical performance of the cells.

EXPERIMENTAL

Materials and Method

Materials for electrode, separator, current collector and electrolyte of supercapacitor were prepared for fabricating symmetrical cells. EFB were used as a precursor to prepare self-adhesive carbon grains (SACG) [15-18], which can be process into activated carbon monolith electrode [19]. PPC (Celgard 3501), ESM and FPW (Whatman 41) were used as nanoporous separator. Stainless steel (316L) and H_2SO_4 were used as current collector and aqueous electrolyte respectively. ESM was obtained from egg shell by treating the egg shell with HCl.

The fibres of EFB were pre-carbonized at low temperature (~280°C), followed by ball milling for 18 h and sieving process to obtain powder of SACG with a particle size of < 106 μm [15,16]. Green monoliths (GMs) from SACG were prepared in a mould with 20 mm diameter using 250 kg cm^{-2} of compression force. The GMs were carbonized at ~800°C under N_2 atmosphere with flow rate 1.5 litre/minutes to produce carbon monoliths (CMs). These CMs were activated with CO_2 for 3 h with a multi-step activation process at ~800°C and a flow rate of 1 litre/minute to produce ACMs [11, 19, 20]. All ACMs electrode were polished until thickness approximately ~0.4 mm. The polished ACMs electrodes were then washed with distilled water to remove the activating agent until it reached pH 7 and dried in the oven for 24 h.

PPC, ESM and FPW were cut into square sheets (2 cm x 2 cm) and the initial weight (W_{dry}) of each nanoporous separator was measured before immersed in 1 M H_2SO_4 electrolyte for five hours. Each nanoporous separator was taken out from the solution and wiped with a tissue paper before it was weighted (W_{wet}) for every one hour. The degree of electrolyte uptake (D_w) were determined from

$$D_W = \frac{W_{wet} - W_{dry}}{W_{dry}} \times 100\%$$

The soaked nanoporous separator were dried at the room temperature by sandwiching between perspex plates holders. Each nanoporous separator was weighted (W_{dry}) for every one hour during the drying process and this process continues until the 4th day. The degree of electrolyte retention (D_R) were determined from $D_R = \frac{W_{wet} - W_{dry}}{W_{wet}} \times 100\%$

Structure of the PPC, EMS and FPW were investigated using X-Ray diffractometer (XRD) (Bruker AXS D8) equipped with CuK_α radiation of 1.5406 Å and nano-pores structural network of PPC, EMS and FPW were investigated using Field Emission Scanning Electron Microscopy (FESEM) (Ziess Supra 55PV).

Electrochemical Characterisation

For electrochemical characterisations, PPC, ESM and FPW nanoporous separators were used in the fabrication of cells A, B and C respectively. The prepared ACMs and all the nanoporous separators were immersed in 1 M H_2SO_4 electrolyte for 24 h before assembling the cells. An electrochemical instrument (Solartron 1286 electrochemical interface and Solartron 1255 HF frequency response analyser) was used to study the performance of the supercapacitor cells using electrochemical impedance spectroscopy (EIS), cyclic voltammetry (CV) and galvanic charge-discharge (GCD) methods. All measurements were carried out at room temperature (25°C).

From the CV data, the specific capacitance (C_{sp}) of the elctrodes was determined using $C_{sp} = \frac{2i}{Sm}$,where i = electric current, S = scan rate and m = weight of electrode. From EIS data, the specific C_{sp} of the electrode was determined using $C_{sp} = \frac{1}{\pi f Z^{"} m}$, where f = frequency, $Z^{"}$ = imaginary impedance at f. The real capacitance (C'), imaginary capacitance $(C^{"})$ as a function of the frequency were analysed using $C"(\omega) = -(Z'(\omega))/(\omega|Z(\omega)|^2)$ and $C' = Z^{Prime}\frac{\omega}{\omega|Z(\omega)|^2}$,where the real impedance (Z'), and imaginary impedance $(Z^{"})$ were obtained from the EIS data [21].

From the GCD data recorded at a current density of 10 mA cm^{-2}, the C_{sp} of the electrodes was determined using $C_{sp} = \frac{2i}{\left(\frac{\Delta V}{\Delta t}\right)m}$, where i = discharge current, Δt = discharge time, and ΔV = voltage [22]. Also from GCD

data, the values of the specific power (P) and specific energy (E) were calculated, respectively, using $P = \frac{V_i}{m}$ and $E = \frac{Vit}{m}$, where i = discharge current, V = voltage excluding the iR_{drop} at the beginning of the discharge, and t is time.

RESULTS AND DISCUSSIONS

Morphology Observation

The micrograph of PPC, ESM and FPW separators are shown in Fig 1. Each nanoporous separator appears to have nanoporous networks which provide a superhighway for promoting diffusion of ions into pores in electrode. In terms of woven fibres, only ESM and FPW composed of interlaced fibres-like structure whereas the structure for PPC is a nonwoven fibres. As can be seen in Fig 1(c), FPW seems to have the highest nanoporous network compared to that of the PPC (Fig 1a) and ESM (Fig 1b). It will be seen in the later section that the highest nanoporous structure of FPW is attributed to the higher electrochemical performance of cell C.

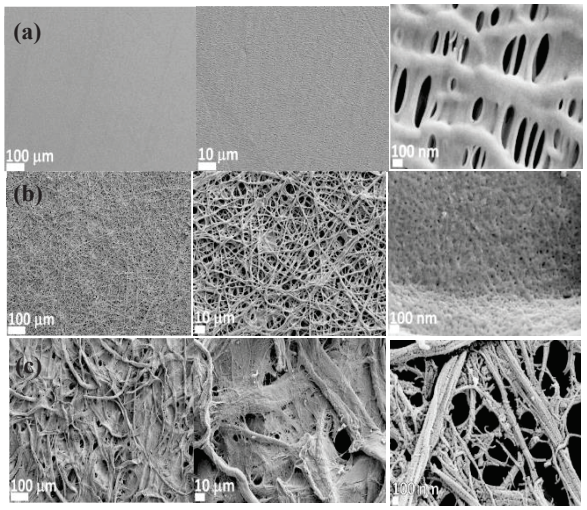

FIGURE 1. FESEM micrographs of (a) PPC (b) ESM and (c) FPW nanoporous separator with different magnification

Structural Analysis

Fig 2 shows the XRD patterns of PPC, ESM and FPW nanoporous separators. It can be seen in this XRD patterns that PPC nanoporous separator (Fig 2a) has the alpha modification type structure represented by the peaks at 14.2° (110), 17.2° (040), 18.9° (130), 21.5° (111) and 22° (130) and the crystal plane of PPC is monoclinic [23]. Fig 2 (b) shows the X-ray diffraction of ESM where the crystalline peaks of $CaCO_3$ (JCPDS 00-005-0586) occurs at 29.5° (104), 36° (110), 39.5° (113), 43.2° (202), 47.5° (018) and 48.5° (116). The ESM structure forms a matrix created by protein fibres bonded to $CaCO_3$ crystals [24] and the broad peak at 21° indicates the amorphous nature of ESM membrane [25]. The XRD peaks observed in Fig 2 (c) at 15°, 16.9° and 23° are belong to cellulose with high crystallinity (JCPDS 00-050-2241). This result is consistent with the fact that FPW was made of paper pulp (containing cellulose) which underwent chemical process meant to remove the amorphous portions of cellulose in paper pulp. These XRD results clearly indicate that the different in separator structure could be correlated well with the different in the nanoporous structure of the nanoporous separators.

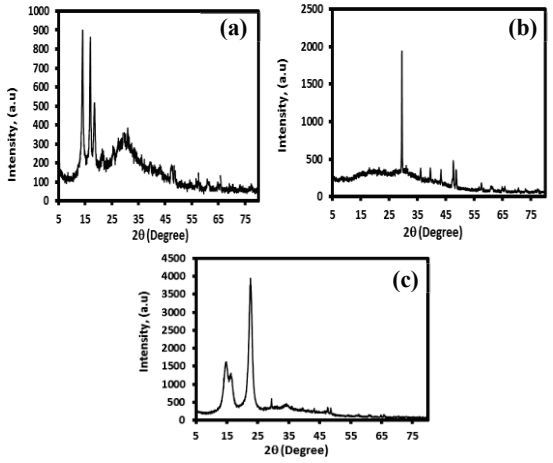

FIGURE 2. XRD pattern for (a) PPC (b) ESM and (c) FPW nanoporous separator

Electrolyte Uptake and Retain properties

The electrolyte uptake profile over a period of 5 hours for each nanoporous separator is shown in Fig 3(a) which shows that FPW has higher electrolyte uptake (140%) compared to ESM (81%) and PPC (57%) separators. Fig 3 (b) shows the electrolyte retention percentage of each nanoporous separator recorded at room temperature over a period of 4 hours. FPW nanoporous separator can retain the highest percentage of electrolyte after 4 hours and the losses were 11% after 4 hours and 100% after 4 days. Meanwhile, a slightly higher loss of electrolyte loss after 4 hours was exhibited by ESM (20%) and PPC (22%). However, on 4th day of drying, ESM showed

the change in colour and their percentage loss were 37%, and for the PPC, the electrolyte loss after 4 days was approximately 20%. As expected, these results were consistent with the pore and nanopore network characteristics of the FPW, ESM and PPC nanoporous separators, as shown by FESEM images in Fig 1.

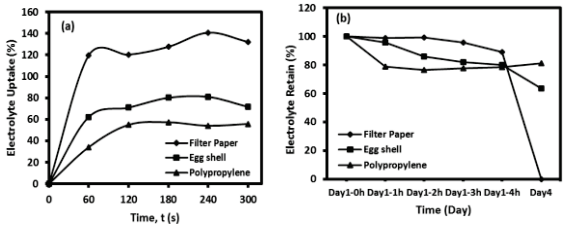

FIGURE 3. (a) Electrolyte uptake (%) PPC, ESM and FPW (b) Electrolyte retention (%) for PPC, ESM and FPW nanoporous separator in 1 M H_2SO_4 electrolyte at room temperature

Electrochemical Performances of Supercapacitor

Fig 4 (a), (b) and (c) shows CV (1 mV s^{-1}), EIS (0.01 – 1 MHz) and GCD (0.01 A cm^{-1}) data obtained from electrochemical measurements. All graphs exhibit a typical shape that represents a satisfactory supercapacitive behaviour of the cells. In Fig 4 (a), cell C shows larger current window compared to cells A and B, however all three cells retain the rectangular like shape at the same scan rate which indicate that all nanoporous separators has the superhighway for ions diffusions. The Nyquist plot Fig 4 (b), i.e. Z" versus Z', show a small semicircle in high frequency region (resistive effect) followed by a Warburg impedance line close to 45° (resistive and increasing effect) in intermediate frequency region and finally ended with a vertical line approaching 90° in low frequency region (dominance capacitive effect). The GCD curves shown in Fig 4 (c) display a typical symmetric charge-discharge performance with a very low ohmic resistance at the potential switching point, indicating that all cells exhibit an excellent electrochemical reversibility and charge-discharge behavior. The values of C_{sp} calculated from Figs 4 (a), (b) and (c) using equations shown in section 2.3, respectively, are shown in Table 1. These three independence electrochemical results are in good agreement in terms of showing a despite small differences in their absolute values.

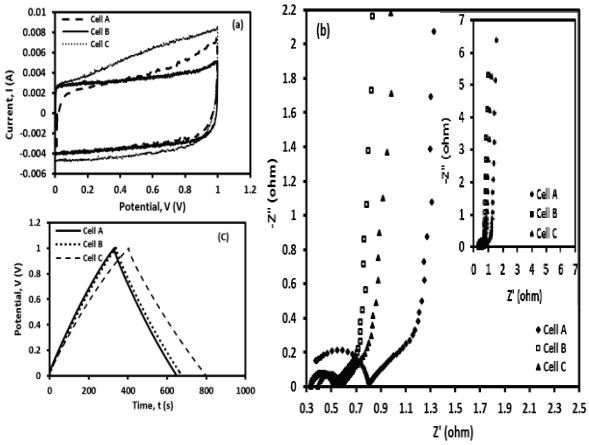

FIGURE 4. (a) Voltammogram data obtained at 1 mV s^{-1}, (b) Nyquist plot, (c) Galvanostatic charge-discharge curves for cell A, B, C

TABLE 1. Specific capacitance of cells A, B and C calculated from EIS, CV and GCD data.

Cells	C_{sp} (F g^{-1}) (EIS)	C_{sp} (F g^{-1}) (CV)	C_{sp} (F g^{-1}) (GCD)
A	91	122	118
B	109	125	123
C	110	180	145

CV data for cells A, B and C measured for a scan rate ranges from 1-100 mV s^{-1} are shown in Fig 5. As the scan rate increase, the data show that the horizontal almost ideal rectangular shape change into tree-leaf shape with its axis tilted toward y-axis. This change occurs because the capacitance is a time-dependent parameter.

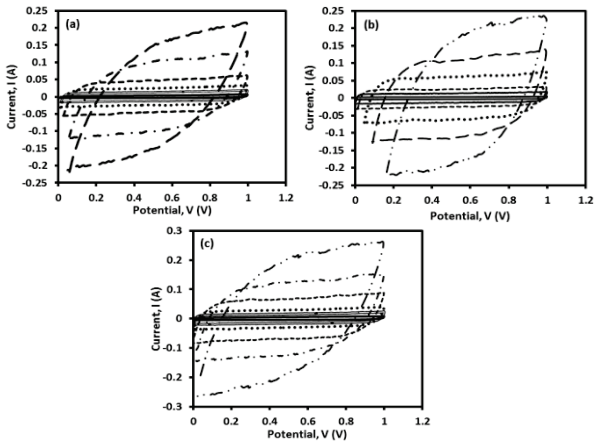

FIGURE 5. Voltammogram obtained at 1-100 mV s^{-1} for (a) cell A, (b) cell B and (c) cell C

Fig 6 (a) and (b) shows the time dependent behaviour of Csp vs. scan rate (from CV) and Csp vs. frequency (from EIS) respectively. These figures shows that when the scan rate increase (or frequency increased), the ions did not have enough time to penetrate into the pore to form efficiently a double layer.

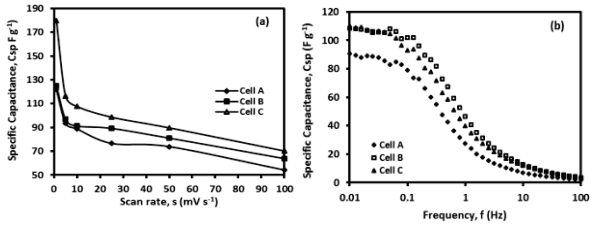

FIGURE 6. (a) Specific capacitance vs. scan rate from CV data (b) Specific capacitance vs. frequency from EIS data for cells A, B and C

The internal resistance, R_s, bulk resistance, R_p, and equivalent series resistance, ESR (R_p-R_s) of the cells determined from Fig 4 (b) are shown in Table 2. The f_o (knee frequency) values and also its corresponding relaxation times, $\tau = \frac{1}{f_0}$ determined from the curves intersection in Bode Plot (Figure 7) are also shown in Table 2. The ESR determined from the voltage loss (iR_{drop}) appears at the beginning of discharge curve are also shown in Table 2. As can be seen in this table, all parameter values for all cells were typical for carbon based supercapacitor, indicating that all cells exhibit a satisfactory capacitive property.

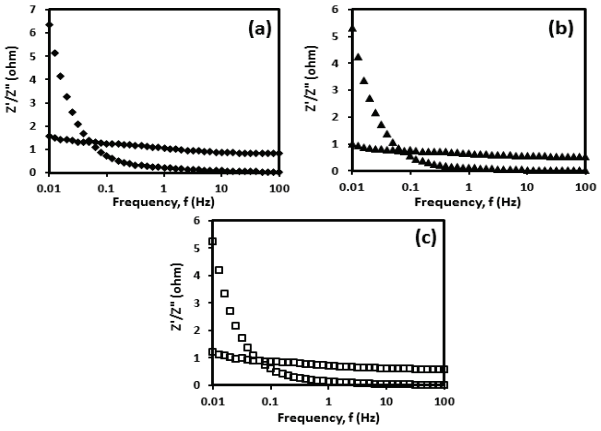

FIGURE 7. Bode plot of (a) cell A, (b) cell B, and (c) cell C

Ragone plot shown in Fig 8 illustrates the variation of the specific energy, E with specific power, P for all cells, and the maximum values of E and P are shown in Table 2. As expected, the P-E relation is depending on the nanoporous characterisation of the nanoporous separators.

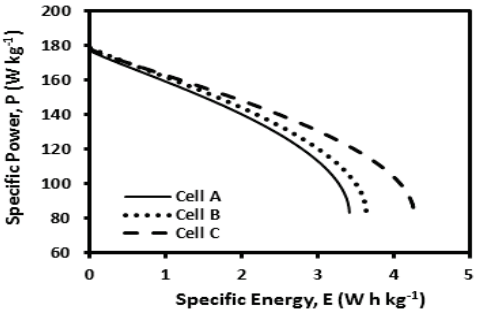

FIGURE 8. Ragone plots for cell A, B and C

CONCLUSION

This study investigated the supercapacitive behavior of supercapacitor cells fabricated using H_2SO_4 electrolyte, activated carbon monolith electrode derived from fibers of oil palm empty fruit bunches, stainless steel current collector and three different types of separators, i.e. FPW, ESM and PPC nanoporous separators. It was found that the FPW nanoporous separator, which composed of higher number of nanopores connected by more open pore networks and therefore capable of absorbing higher amount of electrolyte, can help the cells to exhibit better supercapacitive performance.

ACKNOWLEDGEMENT

We acknowledge the grants from the Universiti Kebangsaan Malaysia (ERGS/1/2012/STG05/UKM/01/2) and the support of CRIM (Centre Research of and Innovation Management). The authors also thank to Mr. Saini for help with the laboratory work.

TABLE 2. The values of R_s, R_p, ESR (EIS), f_o, τ and ESR (GCD)

Cells	R_s (Ω)	R_p (Ω)	ESR (Ω) (EIS)	f_o (Hz)	τ	ESR (Ω) (GCD)	P (W kg^{-1})	E (Wh kg^{-1})
A	0.3723	0.803	0.4306	0.0501	19.952	1.247	177	3.42
B	0.334	0.523	0.1889	0.0794	12.59	0.7705	179	3.64
C	0.3912	0.579	0.188	0.0631	15.848	0.856	178	4.27

REFERENCES

1. Zhang, X., Wang, X., Jiang, L., Wu, H., Wu, C., & Su, J. *J. Power Sources*, **216**, 290–296 (2012).
2. Selvakumar, M., & Bhat, D. K. *Appl. Surf. Sci.*, **263**, 236–241 (2012).
3. Milczarek, G., Ciszewski, A., & Stepniak, I. *J. Power Sources*, **196(18)**, 7882–7885 (2011).
4. Firoz Babu, K., Siva Subramanian, S. P., & Anbu Kulandainathan, M. *Carbohyd. Polym.*, **94(1)**, 487–95 (2013).
5. Basri, N. H., Deraman, M., Kanwal, S., Talib, I. a., Manjunatha, J. G., Aziz, A. a., & Farma, R. *Biomass Bioenerg*, **59**, 370-379 (2013).
6. Dolah, B. N. M., Othman, M. a R., Deraman, M., Basri, N. H., Farma, R., Talib, I. a, & Ishak, M. M. *Journal of Physics: Conference Series*, **431**, 012015 (2013).
7. Farma, R., Deraman, M., Awitdrus, Talib, I. A., Omar, R., Manjunatha, J. G., Dolah, B. N. M. *Int. J. Electrochem. Sci*, **8**, 257–273 (2013).
8. Milani, P., Bettini, L. G., Galluzzi, M., Podesta, A., & Piseri, P. *Carbon*, **59**, 212–220 (2013).
9. Taer, Erman, Deraman, M., Talib, I. A., Umar, A. A., Oyama, M., & Yunus, R. M. *Current Applied Physics*, **10(4)**, 1071–1075 (2010).
10. Farma, R., Deraman, M., Awitdrus, A., Talib, I. a, Taer, E., Basri, N. H., Hashmi, S. a. *Bioresour. Technol.*, **132**, 254–61 (2013).
11. Stepniak, I., & Ciszewski, A. *J. Power Sources*, **195(15)**, 5130–5137 (2010).
12. Yu, H., Tang, Q., Wu, J., Lin, Y., Fan, L., Huang, M., Yu, F. *J. Power Sources*, **206**, 463–468 (2012).
13. Yang, C.-C., Hsu, S.-T., & Chien, W.-C. *J. Power Sources*, **152**, 303–310 (2005).
14. Nyström, G., Strømme, M., Sjödin, M., & Nyholm, L. *Electrochim. Acta*, **70**, 91–97 (2012).
15. Deraman, M, Omar, R., & Harun, A. G. *J. Mater Sci Lett*, **17**, 2059–2060 (1998).
16. Deraman, M, Omar, R., & Zakaria, S. *J. Mater. Sci.*, **7**, 3329–3335 (2002).
17. Deraman, M, & Zakaria, S. *Jpn. J. Appl. Phys.*, **39(12)**, 1236–1238 (2000).
18. Deraman, Mohamad, Zakaria, S., & Murshidi, J. A. *Jpn. J. Appl. Phys.*, **40(5)**, 3311–3314 (2001).
19. Taer, E., Deraman, M., Talib, I. a., Hashmi, S. a., & Umar, A. a. *Electrochim. Acta*, **56(27)**, 10217–10222 (2011).
20. Taer, E, Deraman, M., & Talib, I. *Int. J. Electrochem*, **6**, 3301–3315 (2011).
21. Portet, C., Taberna, P. L., Simon, P., Flahaut, E., & Laberty-Robert, C. *Electrochim. Acta*, **50(20)**, 4174–4181 (2005).
22. Tsay, K.-C., Zhang, L., & Zhang, J. *Electrochim. Acta*, **60**, 428–436 (2012).
23. Shi, Y., Chen, F., Yang, J., & Zhong, M. *Applied Clay Science*, **50(1)**, 87–91 (2010).
24. Ho, W.-F., Hsu, H.-C., Hsu, S.-K., Hung, C.-W., & Wu, S.-C. *Ceramics International*, **39(6)**, 6467–6473 (2013).
25. Li, J., Chiu, K. L., Kwong, F. L., Ng, D. H. L., & Chan, S. L. I. *Current Applied Physics*, **9(6)**, 1438–1444 (2009).